Measurement of Nanofiber Mechanical Flexural Modes Based on Near-Field Scattering

Lijun Song,[1,2,*] Chenxi Wang,[1,2,*] Yudong Hu,[1,2] Jing Zhou,[1,2] Qiang Zhang,[1,2] Chang-Ling Zou,[3,1] Gang Li,[1,2]
Pengfei Zhang,[1,2,†] and Tiancai Zhang[1,2,‡]

[1]*State Key Laboratory of Quantum Optics and Quantum Optics Devices, Institute of Opto-electronics, Shanxi University,
Taiyuan, Shanxi 030006, People's Republic of China*
[2]*Collaborative Innovation Center of Extreme Optics, Shanxi University, Taiyuan, Shanxi 030006, People's Republic of China*
[3]*Key Laboratory of Quantum Information, Chinese Academy of Sciences, University of Science and Technology of China,
Hefei 230026, People's Republic of China*

We systematically investigated the intrinsic mechanical flexural modes of tapered optical fibers (TOFs) with a high aspect ratio up to 3×10^4. Based on the near-field scattering of the hemispherical microfiber tip to the vibrating TOF evanescent field, we detected more than 320 ordered intrinsic mechanical modes through the TOF transmission spectra which was enhanced by 72 dB compared to without near-field scattering. The trend of the vibration amplitude with the mode order was similar to pendulum waves. Our results open a pathway to study the mechanical modes of photonic microstructures-nanostructures that are expected to be used in waveguide QED, cavity optomechanical, and optical sensing.

Nanoscale photonic structures with strong evanescent fields are utilized when pursuing efficient interactions with a surrounding medium and play a key role in advancing quantum optics, quantum information, and quantum-based devices [1–6]. Nanoscale photonic structures with high-aspect ratios have provided an elegant and powerful platform for optomechanics [7] and optical sensing [8]. High-aspect ratio nanostructures offer high sensitivity, wide dynamic range, and low mechanical dissipation [8,9]. Among these nanostructures, tapered optical fibers (TOFs) have attracted special interest because their diameters are close to the optical wavelength and their high aspect ratio can reach 3×10^4. The waist region of a TOF can support a strong transverse evanescent field that is tightly confined, called a nanofiber [10,11]. This means that it can be used as an efficient tool for coupling with the surrounding matter [6]. In addition, there have been significant advances in the realization of hybrid photonic structures, including various types of photonic resonators based on TOFs [11,12]. Thus, TOFs have emerged as a novel and versatile platform [6,13] for nonlinear optics [14], near-field optics [15], quantum optics [13], optomechanics [16,17], and optical sensing [18].

A doubly clamped TOF structure treated as nanostrings can support intrinsic mechanical modes, including flexural, longitudinal, breathing, and torsional modes. Owing to vibrations, it is difficult for TOFs to maintain the polarization and phase of an optical guided field, which results in a decrease in the trapping lifetime [19] of atomic array trapping by a TOF evanescent field [20,21], and limits the stabilization of photonic devices coupled with TOFs [20]. Conversely, the mechanical vibrations of TOFs provide a platform for studying elastic mechanics at the nanoscale and expanding their application in optomechanical technology [22]. It is critical to precisely characterize TOF modes, which is central to many applications ranging from optical sensing to quantum technologies [22–25].

The nanoscale mechanical modes of photonic structures have been achieved by far-field optical methods such as optical interferometry [26], optical scattering [21], and beam deflection [27]. However, as photonic structure dimensions decrease, their measurement accuracy becomes more insensitive and inevitably limited by the optical diffraction limit [28]. Fortunately, near-field optics based on the surface evanescent field of TOFs and cavities can easily break through the optical diffraction limit of light to realize TOF displacement detection [15,21,25]. However, these schemes require high stability and spatial accuracy of the cavities or the TOFs. Moreover, the torsional mode measurement of TOFs by direct mechanical excitation of electrodes and injecting amplitude-modulated light has also been explored experimentally [22–24]. Nevertheless, systematically measuring the complete flexural modes of TOFs has not yet been achieved.

In this Letter, the flexural modes of a TOF with an aspect ratio as high as 3×10^4 are systematically studied for the first time. We propose and demonstrate a novel method for achieving high sensitivity and enhanced measurement for high-order modes. This method is based on the near-field scattering of a TOF caused by a hemispherical microfiber tip (MFT). When the hemispherical MFT extremity is immersed in the evanescent field of TOF, the field distribution could be further extended, leading to an increased scattering loss in transmitted TOF light. The
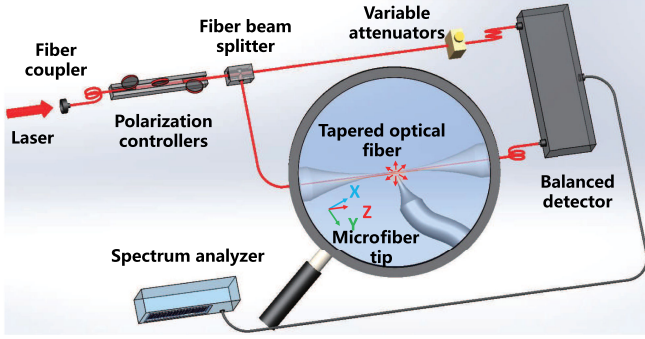
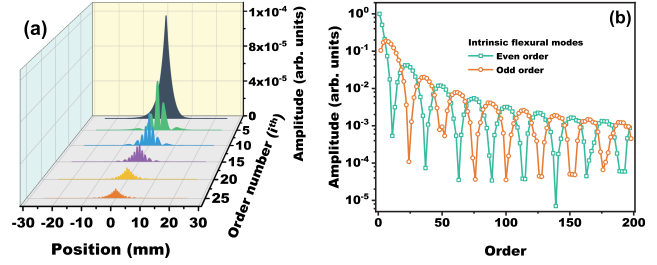FIG. 1. Experimental setup for detecting the TOF flexural modes.

FIG. 2. The TOF flexural modes are simulated with COMSOL Multiphysics. (a) The vibration amplitude (x axis) as a function along the nanofiber axis (z axis) for the 1st, 5th, 10th, 15th, 20th, and 25th order modes. (b) The vibration amplitudes of various order TOF flexural modes at position $z = 0.1$ mm.

scattering loss is sensitive to the gap size between the TOF and MFT [29–31]. The transmission of TOF is affected by the perturbations in the TOF-MFT gap arising from the TOF's flexural vibrations. Under appropriate conditions of MFT diameter and TOF-MFT gap, the TOF flexural vibration can be detected with a high enhancement. Experimentally, we measure the TOF vibration spectrum in high vacuum, which is in good agreement with the numerical simulation results. Furthermore, the MFT-enhanced vibration behavior of TOFs caused by external resonant and off-resonant mechanical excitation is demonstrated. This method of vibration amplitude and profile measurement can be extended to other microstructures-nanostructures [31], such as integrated photonic and MEMS devices.

Figure 1 schematically illustrates the TOF-MFT system for the measurement of TOF flexural modes. The TOF diameter is comparable to the light wavelength; thus, there is a considerable portion of the optical guide mode outside the dielectric in the evanescent field. The evanescent field extending into the surrounding air decreases exponentially with a scale less than half of the wavelength [32]. The flexural modes of the TOF generated by Brownian motion will modulate the TOF-MFT gap size. Once the TOF-MFT gap changes slightly due to the TOF flexural vibration, the TOF transmitted light intensity is modulated. This means that the TOF transmission will follow the perturbations induced by the TOF flexural vibrations. The flexural modes can be detected by measuring and analyzing the spectrum of TOF transmitted light. The TOF transmission can be expressed as

$$T(t) = T_{d_0} + \frac{\partial T}{\partial d} \sum_i \delta d_i(t), \qquad (1)$$

where T_{d_0} is the transmission when the TOF-MFT gap is $d = d_0$. The derivative of $(\partial T/\partial d)$ denotes the relationship between TOF transmission and the gap. This relationship has been simulated numerically and demonstrated experimentally [29]. $\delta d_i(t)$ represents the minute time-dependent displacement of the TOF ith mode.

The TOF flexural modes are simulated using the finite element method with COMSOL Multiphysics version 5.6 (see the Supplemental Material, Sec. I [33]). The TOF profiles used in the simulations are from the measured results of a real TOF (the values are shown in Fig. S2(a) in the Supplemental Material, Sec. I [33]). We conclude and plot the flexural mode amplitude and frequency as a function of the z axis and the mode order, which are shown in Fig. S2(c) of the Supplemental Material, Sec. I [33]. We used simplified formulas to fit them to obtain an approximated numerical expression of the flexural amplitude with various orders along the TOF axis shown in the Supplemental Material, Sec. II [33]:

$$A(i, z) = |A_0(i, z)\cos[K(i, z)z]|, \qquad (2)$$

where $A_0(i, z)$ is the vibration amplitude at the TOF axial position z for the ith order mode, and $K(i, z)$ is the wave number of the ith order mode along the TOF axis.

We plot the vibration amplitude as a function of the z axis for the 1st, 5th, 10th, 15th, 20th, and 25th order modes, which are shown in Fig. 2(a). The phonon number of the TOF vibration mode and vibration amplitude decrease with increasing order. Moreover, the flexural vibration for all the modes is concentrated in the TOF central region (concentrated region), which is approximately 15 mm in length. A larger diameter will cause a smaller vibration amplitude; thus, the TOF vibration amplitude varies with the TOF's tapered profile along its axis. In this model, the size of the touched point between the MFT and the TOF should be less than the MFT size of 37.3 µm, and it is much less than the mechanical wave wavelength from 15 mm to 82.2 µm when the mode order ranges from 1 to 200. Thus, the TOF-MFT system can measure the amplitude of a mechanical wave packet at a single point along the TOF axis. For each order of the wave packet, the vibration amplitudes can be detected simultaneously. Figure 2(b) shows the normalized maximum vibration amplitudes as a function of order when the MFT is at a position of $z = 0.1$ mm. For this position of the MFT, the vibration amplitudes for the even-order (green

open squares) and odd-order (orange open circles) modes exhibit opposite trends with increasing order. This reveals the varying amplitudes for different order modes, which is similar to a typical vibration behavior of pendulum waves [34,35].

The MFT is fabricated by a carbon dioxide laser with a wavelength of 10.6 μm. The fabrication setup and procedures for TOFs and MFTs have been discussed in [29,30]. A TOF glued to a U-shaped quartz holder is positioned on two slip-stick positioners (ANPx51/ANPz51, attocube). The MFT is fixed on a two-axis piezo stage (y and z axes). Thanks to these piezo stages, the MFT extremity can be finely positioned within the TOF evanescent field, and the distance between the MFT and the TOF can be controlled with subnanometer accuracy. In addition, the piezo stage can provide spatial vibration excitation with a certain frequency to the TOF.

A laser (TLB-6716-P, New Focus) with wavelength $\lambda = 852$ nm is coupled into a 50:50 fiber beam splitter. One output is connected to the TOF as a probe light, and another output is coupled into a fiber variable attenuator (VOA850-APC, Thorlabs) as a reference light. The variable attenuator is used to adjust the reference light intensity to keep the two detector inputs equal. During the experiment, the signal light intensity is kept at 20 μW to reduce the heating from scattering and maintain a sufficient signal-to-noise ratio. Two beams are detected by a balanced photodetector (PDB420A, Thorlabs) to achieve a balanced amplification measurement of the flexural modes. The detector signal is input into a spectrum analyzer or an oscilloscope. To reduce the air damping influence on the TOF intrinsic flexural vibration, the system is placed in a high vacuum chamber with pressure as low as 10^{-4} Pa. The light is coupled into the TOF via an optical fiber feedthrough [36]. The TOF transmission reaches more than 95%. The vacuum chamber is fixed on an optical platform with active vibration isolation to reduce low-frequency mechanical vibration from the optical table.

We first measured the intrinsic flexural mode enhancement spectrum of a high-aspect ratio TOF under high vacuum. The enhancement spectrum is the ratio of the enhanced spectrum to the spectral background without the MFT. As shown in Fig. 3(a), the blue curve is the enhancement spectrum with a 20 nm gap between the TOF and the MFT, while the gray curve represents references without scattering loss by the MFT. More than 560 modes are detected; the maximum vibration frequency can reach 1.6 MHz, and the maximum enhancement is 72 dB compared to without near-field scattering. The inset in Fig. 3(a) provides a magnified spectrum with orders ranging from 47th to 50th. We find that there exists a concomitant mode (odd-order mode P_{OV}, green solid circles, or even-order mode P_{EV}, orange solid diamond) next to every main mode (odd-order mode P_{OP}, green open circles, or even-order mode P_{EP}, orange open diamond).
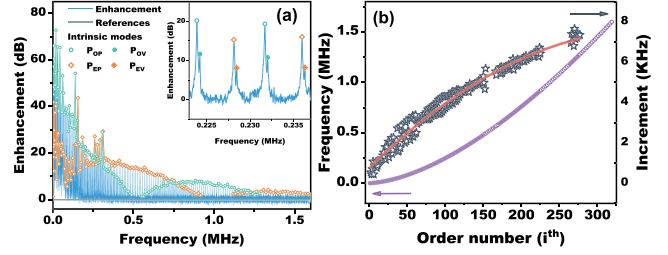

FIG. 3. (a) TOF flexural vibration enhancement spectrum. Inset: enlarged enhancement spectrum of 47th–50th modes. (b) Frequency (purple open circles) and frequency increment (open black stars) of the flexural modes as a function of the mode order; the red curve is the quadratic results.

The concomitant mode and the main mode are orthogonal flexural modes for symmetry breaking of the same order modes due to the TOF radial noncylindrical structure. They are nondegenerate and can be distinguished from the spectrum because of the TOF flexural vibration direction relative to the MFT. The vibration direction causes a distinct vibration amplitude of the two nondegenerate peaks.

From the overall modes with odd order or even order, the flexural vibration amplitude decreases with increasing order, as shown in Fig. 3(a). According to the trend between the frequency and the mode order, approximately 320 order modes can be clearly distinguished. As shown in Fig. 3(b), the TOF vibration frequency (purple open circles) increases nonlinearly with the order. This trend is consistent with the clamped beam flexural modes obtained from the analytical results in the Supplemental Material, Sec. III [33]. However, the axial stress and asymmetry of the TOF also lead to inconsistencies between the measured frequency of the vibration modes and the simulation results. The measured frequencies are higher than the simulated results for the same mode order. The open black stars in Fig. 3(b) indicate the TOF frequency increment of two adjacent orders, and the red curve indicates the quadratic fitting. However, the frequency increment is not strictly linear with the order. The reason is that the concentrated region of the higher-order modes extends slightly into the TOF's tapered region, which can be found in Fig. S2(a) in the Supplemental Material, Sec. I [33], and the extended concentrated region causes a smaller frequency increment.

In addition, the vibration amplitude varies with the mode order in opposite directions for the odd-order and even-order modes, which agrees with the numerical simulation shown in Fig. 2(b). One typical phenomenon is that some modes vanish and are submerged by background noise in frequency ranges from 0.47 MHz to 0.56 MHz, from 0.91 MHz to 1.10 MHz, and from 1.21 MHz to 1.62 MHz. The reason is that the MFT is located near the mode nodes in these frequency ranges. Notably, the MFT modes are not found in the frequency spectrum

experimentally because the TOF vibration amplitudes are 7 orders larger than those of the MFT (see Fig. S5 of the Supplemental Material, Sec. IV [33]). In the frequency range of 0–0.4 MHz, a remarkable fluctuation in the amplitude can be observed because the mechanical vibration from the environment further enhances the TOF intrinsic modes. From these experimental results, it can be seen that the TOF can be affected by vibrations at any frequency.

The influence of external vibration on the TOF is critical when the TOF is used for atom manipulation or coupling with other nanostructures. To demonstrate the TOF response to external mechanical noise, resonant excitation (427 Hz) and off-resonant excitation (550 Hz) are implemented on the TOF. The same sinusoidal modulation intensity is applied to both kinds of excitations, and the modulation frequency is below 1 kHz which is limited by the bandwidth of the piezoelectric transducer of the slipstick positioner. The modulation amplitude is approximately 8 nm, and the modulation direction is perpendicular to the TOF axis (z axis). The vibration spectra with external excitation are shown in Fig. 4(a). The red, cyan, and gray curves represent the resonant excitation, off-resonant excitation, and intrinsic vibration spectra, respectively. The ratio of the vibration amplitude between the excited vibration and the intrinsic vibration is shown in Fig. 4(b). For resonant excitation, the excitation frequency and nonresonant frequency response amplitude increase by more than 36 dB (red arrow) and 20 dB, respectively. Conversely, when off-resonant excitation is applied, the

excitation frequency and nonresonant frequency response amplitude increase by less than 33 dB (blue arrow) and 10 dB, respectively. The maximum displacements of the actual vibration amplitude caused by resonant excitation, nonresonant excitation, and intrinsic vibration are 105.7, 35.2, and 0.4 nm, respectively.

The evolution of flexural vibration in the time domain can qualitatively describe the properties of modes. Figure 4(c) shows the ringdown of resonant excitation (red squares) and off-resonant excitation (cyan hexagons) at a pressure of 1 Pa after the excitation source is suddenly removed. The clifflike drops in the vibration amplitude occur just when the external excitation is stopped for both kinds of excitation. The drop time is too short to measure its spectrum of off-resonant excitation with a measuring resolution time of 10 μs, as shown in the inset of Fig. 4(c). The clifflike drops result from the quick energy decay of the modes at the excited frequencies. Then, the off-resonant excitation presents a slow decay, while the resonant excitation presents double exponential decay, indicating fast decay and slow decay processes. The slow decay is mainly dependent on the energy decay of the adjacent intrinsic mode (638 Hz) induced by the excitation. The black, purple, and green curves in Fig. 4(c) indicate the exponential fittings. During the fast decay for resonant excitation, the vibration energy of all the frequencies decays. However, only intrinsic modes decay during the slow decay for both kinds of excitation; thus, the decay times are the same for the two slow decays. This can be seen in the spectra during the two stages of fast decay and slow decay for the two kinds of excitation shown in Fig. S6 of the Supplemental Material, Sec. V [33]. Additionally, the vibration energy of the off-resonant excitation is higher than the resonant excitation because the frequency of the off-resonant excitation is closer to the adjacent intrinsic mode frequency band (638 Hz) and the weaker response at resonant excitation compared to that at 638 Hz [37].

The influence of pressure on flexural vibration damping is investigated. According to the ringdown, the Q factors of the resonant (red squares) and off-resonant (cyan hexagons) flexural modes' slow decay as a function of the pressure are shown in Fig. 4(d). When the pressure is less than 10^{-2} Pa, the Q factor saturates, which means that the damping effect of the pressure is negligible compared with other mechanical losses. When the pressure is greater than 10^{-2} Pa, the Q factor decreases with increasing pressure. In this case, the mechanical mode damping is dominated by gas damping. The pressure is more than 10^2 Pa, and the damping effect of the pressure on the mechanical modes tends to be saturated. For the fast decay of the resonant excitation (purple diamonds), the Q factor remains constant. More details can be found in Fig. S6 of the Supplemental Material, Sec. V [33]. It is worth noting that oscillation occurs during the decay shown in Fig. 4(c). The oscillation is caused by
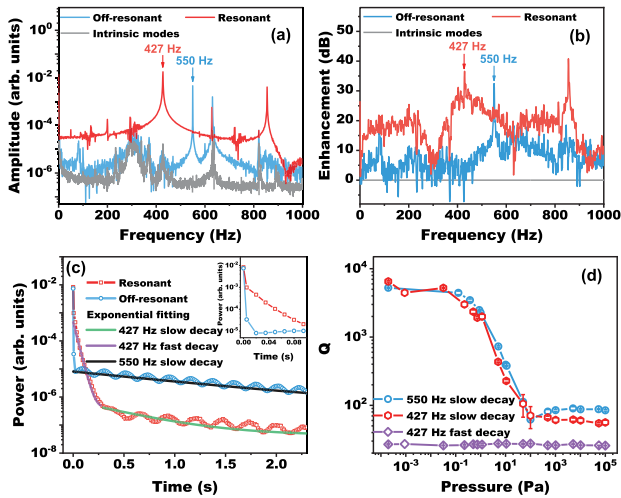

FIG. 4. (a) TOF mechanical vibration spectra with resonant excitation, off-resonant excitation, and intrinsic vibration spectra. (b) The spectra of the enhancement factor. (c) Ringdown of flexural modes with resonant and off-resonant excitation. (d) Q factors as a function of the pressure with resonant, off-resonant modes' slow decay and the fast decay of the resonant excitation. Red and cyan indicate resonant and off-resonant excitation, respectively.

the beating between the two TOF degenerate flexural modes [38].

In conclusion, we have proposed and demonstrated a method to systematically measure the intrinsic flexural modes of a high-aspect-ratio TOF using near-field scattering of the TOF-MFT system. More than 320 orders of the intrinsic flexural modes are discriminated, the maximum vibration frequency can reach more than 1.6 MHz and the maximum enhancement is 72 dB compared to that without near-field scattering. The TOF vibration amplitude decreases with increasing order. For odd-order and even-order modes, the vibration amplitudes vary oppositely, resembling the behavior of pendulum waves. The experimental results are found to be in good agreement with simulation results. The TOF vibration behavior under external resonant and off-resonant mechanical excitation are characterized. In addition, the influence of pressure on the damping of mechanical vibration is investigated. The systematic demonstration of TOF intrinsic flexural modes is significant to the trapping of atomic arrays based on the dipole trap provided by TOFs. This concept and method can be implemented with a variety of microphotonic-nanophotonic structures to either take advantage of the mechanical vibration frequency or to tune it over a larger range while avoiding structural vibration modes [8,31]. It is possible to increase the lifetime of trapped atoms by cooling the TOF [24,39]. This method for measuring high-aspect-ratio nanostructures is expected to be used in waveguide QED [40], cavity optomechanical [17], and optical sensing [41].

---

*These authors contributed equally to this work.
†Corresponding author: zhangpengfei@sxu.edu.cn
‡Corresponding author: tczhang@sxu.edu.cn

[1] S. Slussarenko and G. J. Pryde, Photonic quantum information processing: A concise review, Appl. Phys. Rev. **6**, 041303 (2019).

[2] F. Flamini, N. Spagnolo, and F. Sciarrino, Photonic quantum information processing: A review, Rep. Prog. Phys. **82**, 016001 (2018).

[3] R. K. Ramakrishnan, A. B. Ravichandran, A. Mishra, A. Kaushalram, G. Hegde, S. Talabattula, and P. P. Rohde, Integrated photonic platforms for quantum technology: A review, ISSS J. Micro Smart Syst. **12**, 83 (2023).

[4] D.-Q. Yang, B. Duan, X. Liu, A.-Q. Wang, X.-G. Li, and Y.-F. Ji, Photonic crystal nanobeam cavities for nanoscale optical sensing: A review, Micromachines **11** (2020).

[5] M. Eichenfield, R. Camacho, J. Chan, K. J. Vahala, and O. Painter, A picogram- and nanometre-scale photonic-crystal optomechanical cavity, Nature (London) **459**, 550 (2009).

[6] K. P. Nayak, M. Sadgrove, R. Yalla, F. L. Kien, and K. Hakuta, Nanofiber quantum photonics, J. Opt. **20**, 073001 (2018).

[7] M. Aspelmeyer, T. J. Kippenberg, and F. Marquardt, Cavity optomechanics, Rev. Mod. Phys. **86**, 1391 (2014).

[8] J. Zhou, N. Moldovan, L. Stan, H. Cai, D. A. Czaplewski, and D. López, Approaching the strain-free limit in ultrathin nanomechanical resonators, Nano Lett. **20**, 5693 (2020).

[9] A. Cupertino, D. Shin, L. Guo, P. G. Steeneken, M. A. Bessa, and R. A. Norte, Centimeter-scale nanomechanical resonators with low dissipation, arXiv:2308.00611.

[10] X. Wu and L. Tong, Optical microfibers and nanofibers, Nanophotonics **2**, 407 (2013).

[11] L. Tong, F. Zi, X. Guo, and J. Lou, Optical microfibers and nanofibers: A tutorial, Opt. Commun. **285**, 4641 (2012).

[12] P. Romagnoli, M. Maeda, J. M. Ward, V. G. Truong, and S. Nic Chormaic, Fabrication of optical nanofibre-based cavities using focussed ion-beam milling: A review, Appl. Phys. B **126**, 1 (2020).

[13] P. Solano, J. A. Grover, J. E. Hoffman, S. Ravets, F. K. Fatemi, L. A. Orozco, and S. L. Rolston, *Chapter Seven—Optical Nanofibers: A New Platform for Quantum Optics* (Academic Press, New York, 2017), pp. 439–505, 10.1016/bs.aamop.2017.02.003.

[14] J. Volz, M. Scheucher, C. Junge, and A. Rauschenbeutel, Nonlinear π phase shift for single fibre-guided photons interacting with a single resonator-enhanced atom, Nat. Photonics **8**, 965 (2014).

[15] G. Anetsberger, O. Arcizet, Q. P. Unterreithmeier, R. Rivière, A. Schliesser, E. M. Weig, J. P. Kotthaus, and T. J. Kippenberg, Near-field cavity optomechanics with nanomechanical oscillators, Nat. Phys. **5**, 909 (2009).

[16] Y. L. Li, J. Millen, and P. F. Barker, Simultaneous cooling of coupled mechanical oscillators using whispering gallery mode resonances, Opt. Express **24**, 1392 (2016).

[17] R. Pennetta, S. Xie, R. Zeltner, J. Hammer, and P. S. J. Russell, Optomechanical cooling and self-stabilization of a waveguide coupled to a whispering-gallery-mode resonator, Photonics Res. **8**, 844 (2020).

[18] L. Zhang, J. Lou, and L. Tong, Micro/nanofiber optical sensors, Photonic Sensors **1**, 31 (2011).

[19] D. Hümmer, P. Schneeweiss, A. Rauschenbeutel, and O. Romero-Isart, Heating in nanophotonic traps for cold atoms, Phys. Rev. X **9**, 041034 (2019).

[20] S. M. Spillane, T. J. Kippenberg, O. J. Painter, and K. J. Vahala, Ideality in a fiber-taper-coupled microresonator system for application to cavity quantum electrodynamics, Phys. Rev. Lett. **91**, 043902 (2003).

[21] O. Basarir, S. Bramhavar, G. Basilio-Sanchez, T. Morse, and K. L. Ekinci, Sensitive micromechanical displacement detection by scattering evanescent optical waves, Opt. Lett. **35**, 1792 (2010).

[22] C. Wuttke, G. D. Cole, and A. Rauschenbeutel, Optically active mechanical modes of tapered optical fibers, Phys. Rev. A **88**, 061801(R) (2013).

[23] E. F. Fenton, A. Khan, P. Solano, L. A. Orozco, and F. K. Fatemi, Spin-optomechanical coupling between light and a nanofiber torsional mode, Opt. Lett. **43**, 1534 (2018).

[24] F. Tebbenjohanns, J. Jia, M. Antesberger, A. S. Prasad, S. Pucher, A. Rauschenbeutel, J. Volz, and P. Schneeweiss, Feedback cooling the fundamental torsional mechanical mode of a tapered optical fiber to 30 mK, Phys. Rev. A **108**, L031101 (2023).

[25] U. B. Hoff, G. I. Harris, L. S. Madsen, H. Kerdoncuff, M. Lassen, B. M. Nielsen, W. P. Bowen, and U. L. Andersen, Quantum-enhanced micromechanical displacement sensitivity, Opt. Lett. **38**, 1413 (2013).

[26] C. A. Regal, J. D. Teufel, and K. W. Lehnert, Measuring nanomechanical motion with a microwave cavity interferometer, Nat. Phys. **4**, 555 (2008).

[27] B. Sanii and P. D. Ashby, High sensitivity deflection detection of nanowires, Phys. Rev. Lett. **104**, 147203 (2010).

[28] Q. P. Unterreithmeier, E. M. Weig, and J. P. Kotthaus, Universal transduction scheme for nanomechanical systems based on dielectric forces, Nature (London) **458**, 1001 (2009).

[29] P. Zhang, F. Cheng, X. Wang, L. Song, C.-L. Zou, G. Li, and T. Zhang, Nondestructive measurement of nanofiber diameters using microfiber tip, Opt. Express **26**, 31500 (2018).

[30] P. Zhang, X. Wang, L. Song, C. Wang, G. Li, and T. Zhang, Characterization of scattering losses in tapered optical fibers perturbed by a microfiber tip, J. Opt. Soc. Am. B **37**, 1401 (2020).

[31] L. Wei, X. Kuai, Y. Bao, J. Wei, L. Yang, P. Song, M. Zhang, F. Yang, and X. Wang, The recent progress of MEMS/NEMS resonators, Micromachines **12**, 724 (2021).

[32] F. L. Kien, J. Q. Liang, K. Hakuta, and V. I. Balykin, Field intensity distributions and polarization orientations in a vacuum-clad subwavelength-diameter optical fiber, Opt. Commun. **242**, 445 (2004).

[33] See Supplemental Material at http://link.aps.org/supplemental/10.1103/PhysRevLett.132.033801 for numerical simulations of TOF flexural modes, amplitudes of various orders along the TOF axis, intrinsic doubly clamped string eigenfrequencies of the flexural modes, and TOF behaviors with mechanical modulation.

[34] J. A. Flaten and K. A. Parendo, Pendulum waves: A lesson in aliasing, Am. J. Phys. **69**, 778 (2001).

[35] C. Liang, W. Ke, M. Fu, C. Wang, and X. Chen, An undergraduate experiment of wave motion using a coupled-pendulum chain, Am. J. Phys. **83**, 389 (2015).

[36] E. R. Abraham and E. A. Cornell, Teflon feedthrough for coupling optical fibers into ultrahigh vacuum systems, Appl. Opt. **37**, 1762 (1998).

[37] D. Bothner, S. Yanai, A. Iniguez-Rabago, M. Yuan, Y. M. Blanter, and G. A. Steele, Cavity electromechanics with parametric mechanical driving, Nat. Commun. **11**, 1589 (2020).

[38] D. H. Zanette, Energy exchange between coupled mechanical oscillators: Linear regimes, J. Phys. Commun. **2**, 095015 (2018).

[39] D. Su, Y. Jiang, P. Solano, L. A. Orozco, J. Lawall, and Y. Zhao, Optomechanical feedback cooling of a 5 mm-long torsional mode, arXiv:2301.10554.

[40] A. S. Sheremet, M. I. Petrov, I. V. Iorsh, A. V. Poshakinskiy, and A. N. Poddubny, Waveguide quantum electrodynamics: Collective radiance and photon-photon correlations, Rev. Mod. Phys. **95**, 015002 (2023).

[41] L. Tong, Micro/nanofibre optical sensors: Challenges and prospects, Sensors (Switzerland) **18**, 903 (2018).